Stability Analysis of Dual Active Bridge Converter with Input Filter and Constant Power Load

Yao Sun, *Member, IEEE*, Shutian Yan, *Student Member*, Guo Xu, *Member, IEEE*, Guoliang Deng, *Student Member*, and Mei Su, *Member*, *IEEE*

***Abstract*—Fast scale stability of Dual active bridge (DAB) converter with input filter under constant power load (CPL) is analyzed in this paper. Since the commonly used reduced-order average model is not effective to accurately describe the dynamic behavior of DAB converter, a discrete-time model is established. The bifurcation points of the system are predicted by using bifurcation diagrams. In addition, Poincaré map theory and the Jacobian matrix of the system are used for bifurcation analysis. The eigenvalue locis of Jacobian matrix are carried. Serval Hopf bifurcations and a saddle-node bifurcation, which are predicted by the eigenvalue locis, have been found in the converter. The influence of system parameters on the stability of the system is explained in detail. It is found that high output voltage bandwidth, input filter and light-load are the main causes of instability in this system. To stabilize the converter, a proper feedback control is presented. In addition, stable boundaries are given to help to avoid instability. All the findings have been verified by simulation and experimental results.**

***Index Terms*—Dual active bridge (DAB) converter, discrete-time modeling, nonlinear dynamics, stability analysis, constant power load (CPL), input filter.**

I. INTRODUCTION

Some nonlinear behaviors such as subharmonic oscillation, Hopf bifurcation, saddle node bifurcation and period-doubling bifurcation can be found in power electronic systems [1-2]. DAB converter, as a typical bidirectional DC/DC converter, is widely used in distributed generation systems and electric vehicles due to its characteristics of isolation, two-way power transmission, symmetry, high efficiency and high power density [3]. Like other power converters, DAB may also exhibit some nonlinear behaviors [4-7]. These unexpected behaviors will degrade system performance and affect system security [1]. Therefore, it is necessary to predict these behaviors and avoid them in practical applications.

To predict these complex behaviors, proper modeling methods are essential. The conventional state-space averaging method [8] is widely used to model power electronic systems such as buck and boost converters [9], where ripples of voltages or currents are negligible. However, because the inductor current of DAB is pure AC current and the small ripples hypothesis no longer holds for DAB, other proper methods should be used. Generalized averaging method is proposed in [10-11], which considers multiple frequency components instead of only the dc component like in conventional state-space averaging method. This method can be used to investigate the small-signal behavior of DAB converter [12-13], but it is too complicated to guarantee its accuracy. Since the time scale of the leakage inductance current is small, the reduced-order average model of DAB based on singular perturbation theory is obtained [14-15]. In addition, the reduced-order average model of DAB taking effect of magnetizing inductance and core losses into accounting is built [16-17]. However, the reduced average models are only effective at low-frequency, because they completely ignore the dynamics of the leakage inductance current. Thus, they cannot be applied to predict fast-scale stability issues.

Discrete-time models are a reliable solution to study the dynamic behavior of switching converters [18]. A discrete-time small signal model of DAB converter is established, which could predict the small-signal frequency response up to one-third of the switching frequency [19]. Based on the semi-periodic symmetry property of state variables, a discrete time model of DAB, which incorporates behavior during zero-voltage switching intervals are proposed [20-22]. Based on approximate discrete-time models, A discrete-time framework was proposed to analyze the stability of DAB converter at high frequency [30]. In addition, in order to simplify the iteration of complex exponential matrix, a bilinear discrete time model of DAB converter is proposed, and nonlinear behavior is studied [4-5]. In [7], a decomposition discrete time model is proposed to simplify the complex exponential matrix and the effect of time delay is investigated.

In practice, it is common to add LC input filters before the power stage to suppress the noise and surge from the front stage power supply and to decrease the interference caused by

Manuscript received Dec 9, 2020; revised Mar 10, 2021 and May 9, 2021; accepted Jun 18, 2021. This work was supported in part by the science and technology innovation Program of Hunan Province under Grant 2020RC4002, the National Natural Science Foundation of China under Grant 61933011 and 51807206, the Major Project of Changzhutan Self-dependent Innovation Demonstration Area under Grant 2018XK2002, the Project of Innovation-driven Plan in Central South University under Grant 2019CX003. *(Corresponding author: Guo Xu).*

Yao Sun, Shutian Yan, Guo Xu, Guoliang Deng and Mei Su are with the Hunan Provincial Key Laboratory of Power Electronics Equipment and Gird, School of Automation, Central South University, Changsha 410083, China (E-mail: yaosuncsu@gmail.com; yanshutian@csu.edu.cn; xuguocsu@csu.edu.cn; dengguoliang@csu.edu.cn; sumeicsu@csu.edu.cn).

This article has been accepted for publication in a future issue of this journal, but has not been fully edited. Content may change prior to final publication. Citation information: DOI 10.1109/JESTIE.2021.3093249, IEEE Journal of Emerging and Selected Topics in Industrial Electronics

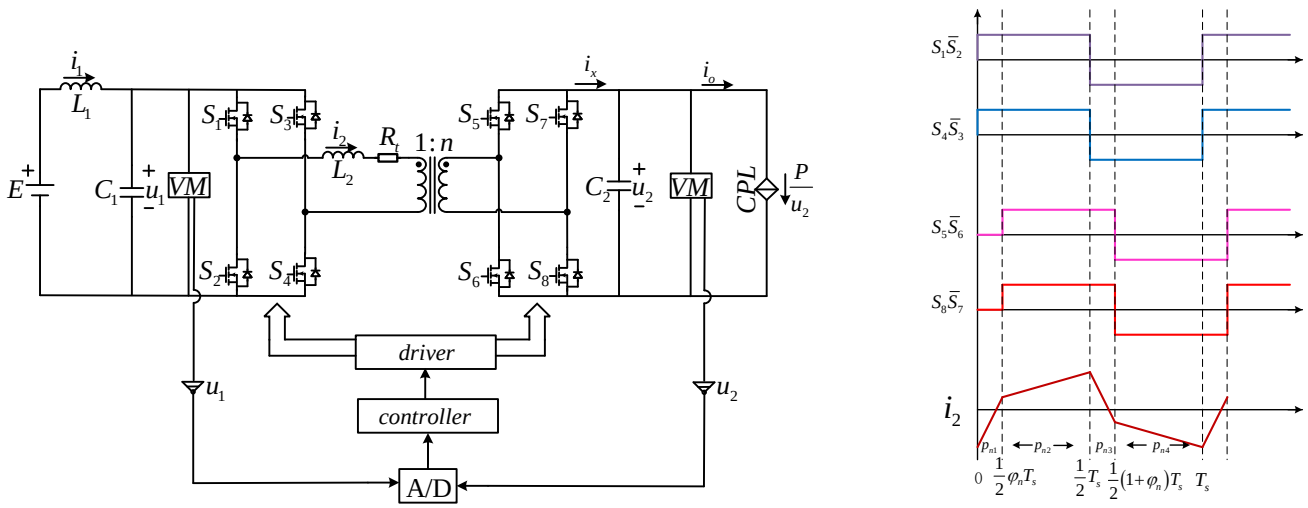

Fig. 1. (a)Diagram of a digitally controlled DAB converter (b) State variables iteration relationship

harmonic current to go back to the power supply. However, some researchers point out that the input filter can cause stability problems [23]. Moreover, constant power loads (CPL) are very common nowadays. CPL results in negative impedance and the negative impedance characteristics of CPL is a root cause of instability [24-27].

In this paper, stability analysis of DAB converter system with input filter and constant power load is carried out. To the best of my knowledge, the effects of input filter and constant power load on stability of DAB are not considered in the past. The discrete-time model of the DAB is established, which includes the digital control delay and sample-and-hold process, input filters and CPL. Bifurcation diagrams are used to predict all the possible bifurcation of the system. In addition, to guide the controller and circuit design, eigenvalue analysis of Jacobian matrix was carried out to study the influence of all kinds of control parameters on stability boundary.

The remainder of this article is organized as follows. Section 2 gives a description of the digitally controlled DAB converter. Besides, a discrete-time model of the studied system is established. In Section 3, The influence of several parameters on the stability of the DAB converter, and the boundary of the stability curve is obtained. In Section 4 and 5, simulation and experimental results are given to verify the theoretical analysis. Finally, Section 6 gives conclusions.

II. System Description And Discrete-Time Model

A. System Description

The DAB converter investigated in this work is depicted in Fig. 1(a). It is composed of an input LC filter, DAB converter, CPL and digital controller. The input LC filter is used to meet the requirements of the power quality at the input. The DAB converter consists of a high-frequency transformer with a ratio of 1: n and a pair of H-bridge converters.

For the sake of simplicity, single-phase shift (SPS) modulation is employed for DAB converter [28]. And its operating waveforms and gate driving signals are illustrated in Fig. 1(b), where T_s is the switching period and the switching frequency $f_s=1/(T_s)$. As illustrated in Fig. 1(b), the DAB converter goes through four stages within one switching cycle according to the ON/OFF state of all switching devices. φ is the phase-shifting angle of the controller output. P is the power of the CPL.

Sub-Period 1 p_{n1}: S_1, S_4, S_6, S_7 are ON; S_2, S_3, S_5, S_8 are OFF;
Sub-Period 2 p_{n2}: S_1, S_4, S_5, S_8 are ON; S_2, S_3, S_6, S_7 are OFF;
Sub-Period 3 p_{n3}: S_2, S_3, S_5, S_8 are ON; S_1, S_4, S_6, S_7 are OFF;
Sub-Period 4 p_{n4}: S_2, S_3, S_6, S_7 are ON, S_1, S_4, S_5, S_8 are OFF.

The negative impedance characteristic of the constant power load will cause the divergence of the system, so the damping of the system needs to be considered. Virtual impedance control is considered as a suitable method to solve the stability problem caused by CPL. A digital controller is designed for the DAB. Its control block diagram is shown in Fig. 2, which includes a proportional integral (PI) control for output voltage regulation and a proportional control for stabilization. The phase shift angle φ is the output of the controller and it ranges between 0 to 0.5. The delay block represents computation time delay T_d which is a sampling period. u_1^* and u_2^* are the references of input voltage u_1 and output voltage u_2.

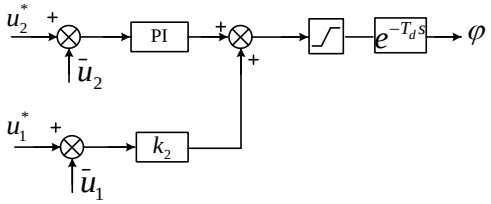

Fig. 2 Control block diagram

B. Reduced-order Average Model

If the DAB is treated as a DC transformer and assumed to be lossless, a reduced-order average model of DAB converter is built as follows [16].

This article has been accepted for publication in a future issue of this journal, but has not been fully edited. Content may change prior to final publication. Citation information: DOI 10.1109/JESTIE.2021.3093249, IEEE Journal of Emerging and Selected Topics in Industrial Electronics

$$\begin{cases} L_1 \dfrac{di_1}{dt} = E - u_1 \\ C_1 \dfrac{du_1}{dt} = i_1 - \dfrac{P_0}{u_1} \\ C_2 \dfrac{du_2}{dt} = \dfrac{P_0}{u_2} - \dfrac{P}{u_2} \end{cases} \tag{1}$$

where P_o is the average power flowing through the DAB converter, which is expressed as

$$P_o = \frac{u_1 u_2}{2nL_2 f_s}\varphi(1-\varphi) \tag{2}$$

where n is transformer ratio. This model is simple and widely used, but it is effective only in the range of low frequency because it neglects the dynamic behavior of the inductance current of DAB. To accurately predict some nonlinear fast-scale behavior of the power converter, more accurate models are needed.

C. Switching Function Model

Assume that the switches of the same bridge of the DAB are switched in a complementary manner. According to Fig. 1, the switching function model of the DAB converter is expressed as follows.

$$\begin{cases} L_1 \dfrac{di_1}{dt} = E - u_1 \\ C_1 \dfrac{du_1}{dt} = i_1 - (s_1 - s_3) i_2 \\ L_2 \dfrac{di_2}{dt} = (s_1 - s_3) u_1 - (s_5 - s_7)\dfrac{u_2}{n} - i_2 R_t \\ C_2 \dfrac{du_2}{dt} = (s_5 - s_7)\dfrac{i_2}{n} - \dfrac{P}{u_2} \end{cases} \tag{3}$$

This is an accurate model, but it is not suitable for controller design and stability analysis in continuous time domain due to the unique nonlinear properties of the switching functions in (3).

D. Discrete-time Model for Power Stage Circuit

According to Fig. 1(b), there are 4 switching states in total during a control period. Using the approach in [29] to linearize CPL around its operating point. Therefore, on the basis of (3) the corresponding state-space description is expressed as follows

$$\frac{dx}{dt} = A_j x + B_j \qquad j = \{1,2,3,4\} \tag{4}$$

where state vector $x = [i_1\ u_1\ i_2\ u_2]^T$; matrices A_j and B_j are shown below:

$$A_1 = \begin{bmatrix} 0 & -\frac{1}{L_1} & 0 & 0 \\ \frac{1}{C_1} & 0 & -\frac{1}{C_1} & 0 \\ 0 & \frac{1}{L_2} & -\frac{R_t}{L_2} & \frac{1}{nL_2} \\ 0 & 0 & -\frac{1}{nC_2} & \frac{P}{C_2(u_2)^2} \end{bmatrix} \quad A_2 = \begin{bmatrix} 0 & -\frac{1}{L_1} & 0 & 0 \\ \frac{1}{C_1} & 0 & -\frac{1}{C_1} & 0 \\ 0 & \frac{1}{L_2} & -\frac{R_t}{L_2} & -\frac{1}{nL_2} \\ 0 & 0 & \frac{1}{nC_2} & \frac{P}{C_2(u_2)^2} \end{bmatrix}$$

$$A_3 = \begin{bmatrix} 0 & -\frac{1}{L_1} & 0 & 0 \\ \frac{1}{C_1} & 0 & \frac{1}{C_1} & 0 \\ 0 & -\frac{1}{L_2} & -\frac{R_t}{L_2} & -\frac{1}{nL_2} \\ 0 & 0 & \frac{1}{nC_2} & \frac{P}{C_2(u_2)^2} \end{bmatrix} \quad A_4 = \begin{bmatrix} 0 & -\frac{1}{L_1} & 0 & 0 \\ \frac{1}{C_1} & 0 & \frac{1}{C_1} & 0 \\ 0 & -\frac{1}{L_2} & -\frac{R_t}{L_2} & \frac{1}{nL_2} \\ 0 & 0 & -\frac{1}{nC_2} & \frac{P}{C_2(u_2)^2} \end{bmatrix}$$

$$B_1 = B_2 = B_3 = B_4 = \begin{bmatrix} E/L_1 & 0 & 0 & -2P/(C_2 u_2) \end{bmatrix}$$

Clearly, the equation in (4) for each switching states is a nonlinear differential equation.

To obtain the discrete model of the DAB converter, assume that the initial conditions of the state variables at the beginning of the n^{th} cycle is x_n, and the $n+1^{th}$ cycle is x_{n+1}. The key to the discrete modeling is to find the mapping between x_n and x_{n+1}. According to the analysis before, the mapping could be solved from Fig. 3.

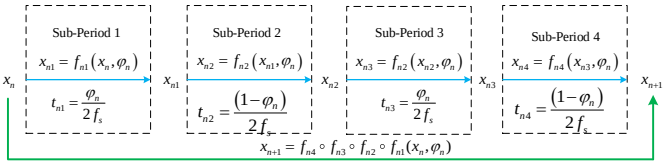

Fig. 3 Mapping from x_n to x_{n+1}.

As is well-known, if A_j and B_j in (4) are constant coefficient matrices, it is easy to get the analytic solution of (4). Thus, for simplicity, dynamic equation (5) is modified as follows without loss of much accuracy.

$$\frac{dx}{dt} = \bar{A}_j x + \bar{B}_j \qquad j = \{1,2,3,4\} \tag{5}$$

where $\bar{A}_j$ and $\bar{B}_j$ are obtained by replacing u_2 in A_j and B_j with the U_2 which is the steady value of u_2.

According to Fig. 3, the large-signal discrete-time model of the system in one switching cycle is written as

$$x_{n+1} = f_{n4}\left(f_{n3}\left(f_{n2}\left(f_{n1}\left(x_n, \varphi_n\right), \varphi_n\right), \varphi_n\right), \varphi_n\right) \tag{6}$$

where

$$\begin{cases} x_{n1} = f_{n1}(x_n, \varphi_n) = e^{\bar{A}_1 t_{n1}} x_n + \psi_1 \\ x_{n2} = f_{n2}(x_{n1}, \varphi_n) = e^{\bar{A}_2 t_{n2}} x_{n1} + \psi_2 \\ x_{n3} = f_{n3}(x_{n2}, \varphi_n) = e^{\bar{A}_3 t_{n3}} x_{n2} + \psi_3 \\ x_{n4} = f_{n4}(x_{n3}, \varphi_n) = e^{\bar{A}_4 t_{n4}} x_{n3} + \psi_4 \end{cases}$$

This article has been accepted for publication in a future issue of this journal, but has not been fully edited. Content may change prior to final publication. Citation information: DOI 10.1109/JESTIE.2021.3093249, IEEE Journal of Emerging and Selected Topics in Industrial Electronics

$$\begin{cases} t_{n1} = t_{n3} = \varphi_n T_s / 2 \\ t_{n2} = t_{n4} = (1-\varphi_n) T_s / 2 \end{cases}$$

$$\begin{cases} \psi_1 = \int_0^{t_{n1}} e^{\bar{A}_1 t} \bar{B}_1 dt \\ \psi_2 = \int_0^{t_{n2}} e^{\bar{A}_2 t} \bar{B}_2 dt \\ \psi_3 = \int_0^{t_{n3}} e^{\bar{A}_3 t} \bar{B}_3 dt \\ \psi_4 = \int_0^{t_{n4}} e^{\bar{A}_4 t} \bar{B}_4 dt \end{cases}$$

After algebraic manipulations, (6) is rewritten as

$$x_{n+1} = F_1(\varphi_n) x_n + G(\varphi_n) \tag{7}$$

where

$$F_1(\varphi_n) = e^{A_4 t_{n4}} e^{A_3 t_{n3}} e^{A_2 t_{n2}} e^{A_1 t_{n1}}$$

$$G(\varphi_n) = e^{A_4 t_{n4}} e^{A_3 t_{n3}} e^{A_2 t_{n2}} \psi_1 + e^{A_4 t_{n4}} e^{A_3 t_{n3}} \psi_2 + e^{A_4 t_{n4}} \psi_3 + \psi_4$$

Until now, a nonlinear large-signal discrete-time model of DAB under open-loop control has been obtained.

E. Discrete-time Model for Digital Controller

The schematic diagram of the proposed control is shown in Fig. 2. Take into account the digital controller's delay T_d, its continuous domain model is expressed as

$$\varphi = e^{-T_d s}[(k_p + \frac{k_i}{s})(u_2^* - u_2) + k_2(u_1^* - u_1)] \tag{8}$$

By forward Euler method, the discrete–time model of (8) is expressed as

$$\begin{cases} \varphi_{n+1} = k_p(u_2^* - E_4 x_n) + g_{n+1} + k_2(u_1^* - E_2 x_n) \\ g_{n+1} = k_i T_s(u_2^* - E_4 x_n) + g_n \end{cases} \tag{9}$$

where E_2 = [0 1 0 0] and E_4 = [0 0 0 1]. k_p is the proportional coefficient and k_i is the integral coefficient in the PI controller shown in Fig. 2. g is integral part of the PI controller. The subscript n represents n^{th} modulation periods.

By combining (7) and (9), the discrete-time model under the digital control is obtained as

$$X_{n+1} = F(X_n) \tag{10}$$

where $X_n = [x_n^T \ \varphi_n \ g_n]^T$ and $F(X_n)$ is expressed as:

$$F(X_n) = \begin{pmatrix} F_1(\varphi_n) x_n + G(\varphi_n) E \\ (k_p + k_i T_s)(u_2^* - E_4 x_n) + g_n + k_2(u_1^* - E_2 x_n) \\ k_i T_s(u_2^* - E_4 x_n) + g_n \end{pmatrix} \tag{11}$$

III. Stability Analysis of DAB Converter

As bifurcations will bring undesired noise, power losses, harmonics and even damage to power converters, all kinds of bifurcations should be avoided in the control design process. Therefore, stability analysis is essential for DAB converters.

A. Bifurcation diagram analysis

TABLE I

Parameters	Value	Parameters	Value
E	30V	R_t	0.1Ω
L_1	0.13mH	n	1.9
C_1	30uF	C_2	400uF
L_2	35uH	U_o^*	60V
f_s	20kHz	T_d	50μs
k_i	400		

Bifurcation diagrams show the values visited or approached asymptotically as a function of a bifurcation parameter in the system. The purpose of the diagram is to display qualitative information about equilibria. In this section, three bifurcation diagrams are plotted using k_p, k_2 and P as the bifurcation parameters. Note that the values of i_2 shown in bifurcation diagrams are the sampled values at the start point of each modulation period.

k_p is an important parameter which is related to output voltage regulation. The larger k_p is, the faster the output voltage responds. However, a large k_p may lead to instability. Take the case that P=100W and k_2=-0.017 as an example, the bifurcation diagram using k_p *as* the bifurcation parameter is plotted and shown in Fig. 4. The vertical axis represents current i_2 and the

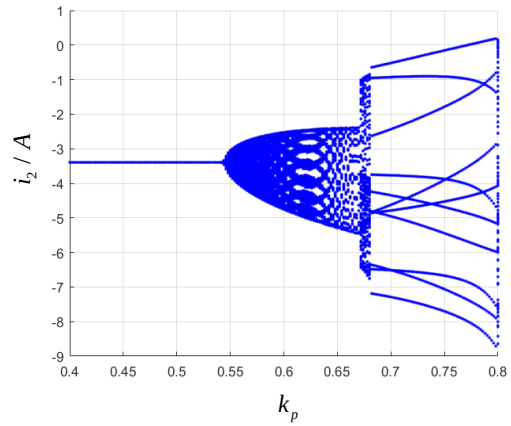

Fig. 4 Bifurcation diagram for i_2 using k_p as the bifurcation parameter(P=100W, k_2=-0.017)

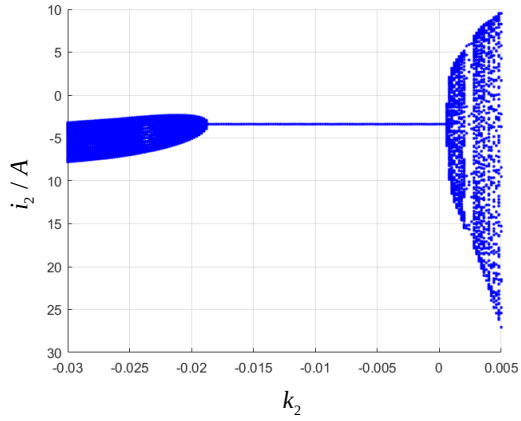

Fig. 5 Bifurcation diagram for i_2 using k_2 as the bifurcation parameter. (P=100W, k_p =0.45)

This article has been accepted for publication in a future issue of this journal, but has not been fully edited. Content may change prior to final publication. Citation information: DOI 10.1109/JESTIE.2021.3093249, IEEE Journal of Emerging and Selected Topics in Industrial Electronics

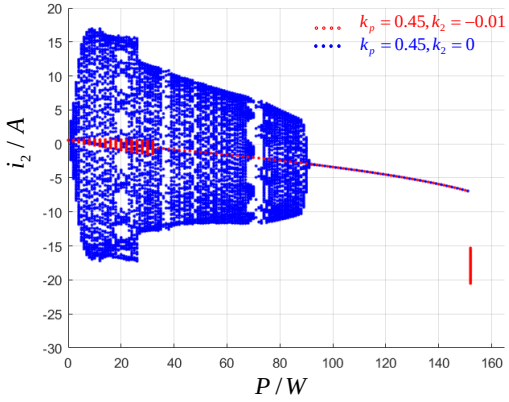

Fig. 6 Bifurcation diagram for i_2 using P as the bifurcation parameter. k_p=0.45, k_2=-0.01 and k_p=0.45, k_2=0

horizontal axis is k_p. It is found that the first bifurcation occurs at k_p =0.53. The system is stable when k_p <0.53. It is worth noting that the parameters used for plotting bifurcation diagrams are listed in Table I.

Due to the presence of input filter, k_2 is designed to increase the damping of the system. The bifurcation diagram, when P=100W and k_p =0.45, using k_2 *as* the bifurcation parameter is shown in Fig. 5. It is found that the value range of k_2 is between -0.017 and 0 for stabilization.

Constant power load is a root cause of instability. Therefore, the bifurcation diagram using P *as* the bifurcation parameter is also plotted and shown in Fig. 6. As can be seen in Fig.6, the red case show that the converter loses its stability under light load conditions, and the bifurcation occurs at P =90W when k_2=0. However, in the red case, the bifurcation occurs at P =34W when k_2=-0.01. The comparison between red and blue cases indicates that without feedback control k_2, the system would have a wider range of instability under light load.

B. *Jacobian Matrix analysis*

The Jacobian plays an important role in the study of dynamical systems. Bifurcations of the system can be accurately predicted by analyzing the eigenvalues of the Jacobian matrix of the discrete-time map in (12). If all the eigenvalues are within the unit circle, the system is stable. One of the ways to locate subharmonic oscillation boundary is by solving the following characteristic equation.

$$\det(J - \lambda I) = 0 \tag{12}$$

where $J = \partial F / \partial X \mid_{X=\bar{X}}$.

Taking parameter k_p as an example to analyze the stability and bifurcation of the system, the eigenvalue loci of characteristic equation are shown in Fig. 7. The maximal absolute values of the eigenvalues around the bifurcation point are listed in Table II. It is found that the eigenvalues move out the unit circle when k_p is increased. Hopf bifurcation is a local bifurcation where a pair of complex conjugate eigenvalues cross the unit cycle [2]. Therefore, a Hopf bifurcation occurs when k_p=0.54 in the system.

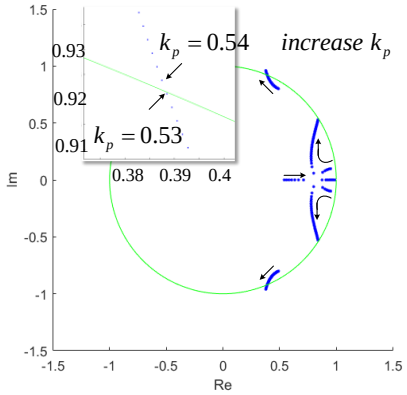

Fig. 7. Loci of eigenvalues by varying k_p. (P=100W and k_2=-0.017)

TABLE II

k_p	Maximal absolute value of eigenvalues	Remarks
0.49	0.977	Stable
0.5	0.9826	Stable
0.51	0.9882	Stable
0.52	0.9938	Stable
0.53	0.9994	Stable
0.54	1.005	Unstable
0.55	1.0106	Unstable

Similarly, the eigenvalue loci of the system by changing k_2 from -0.02 to 0.005 are plotted and shown in Fig. 8, where P=100W and k_p =0.45. According to the moving directions of the eigenvalue loci shown in Fig. 8, it can be found that both too large and too small k_2 will lead to instability. Therefore, there are two bifurcation points for k_2 and both of them are Hopf bifurcation. The maximal absolute values of the eigenvalues around the bifurcation points are listed in Table III and IV. Furthermore, the bifurcation points calculated based on Jacobian matrix are in agreement with the results from bifurcation diagram.

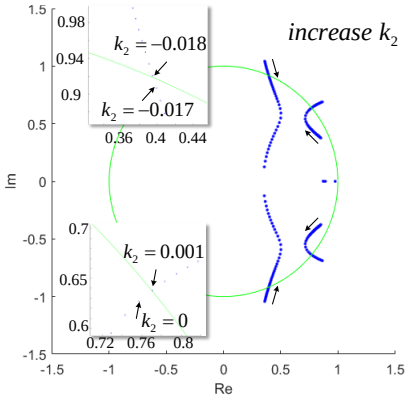

Fig. 8 Loci of eigenvalues by varying k_2. (P=100W and k_p=0.45)

TABLE Ⅲ

k_2	absolute value of eigenvalues	Remarks
-0.013	0.9410	Stable
-0.014	0.9532	Stable
-0.015	0.9653	Stable
-0.016	0.9772	Stable
-0.017	0.9890	Stable
-0.018	1.0007	Unstable
-0.019	1.0122	Unstable

This article has been accepted for publication in a future issue of this journal, but has not been fully edited. Content may change prior to final publication. Citation information: DOI 10.1109/JESTIE.2021.3093249, IEEE Journal of Emerging and Selected Topics in Industrial Electronics

TABLE IV

k_2	absolute value of eigenvalues	Remarks
-0.004	0.9713	Stable
-0.003	0.9745	Stable
-0.002	0.9814	Stable
-0.001	0.9862	Stable
0	0.9911	Stable
0.001	1.0007	Unstable
0.002	1.0122	Unstable

The eigenvalue loci of the system by changing P on the intervals [15, 40] and [150, 170] are plotted and shown in Fig. 9 (a) and (b), respectively, where k_p =0.45 and k_2=-0.01. The maximal absolute values of the eigenvalues around the bifurcation points are listed in Table V and VI. According to the moving directions of the eigenvalue loci in Fig. 9 (a), the eigenvalue loci move out of the unit circle with the decrease of output power P. When P = 34W, the eigenvalue loci cross the unit circle, and a Hopf bifurcation occurs in the system. In addition, Fig. 9 (b) shows the moving directions of the eigenvalue loci with the increase of output power. As seen that an eigenvalue crosses the unit circle from a positive real axis when P=163W, a saddle-node bifurcation occurs in the system.

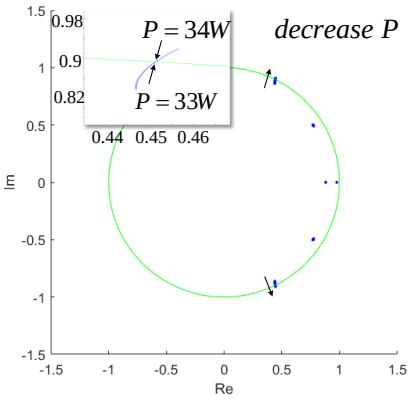

(a)

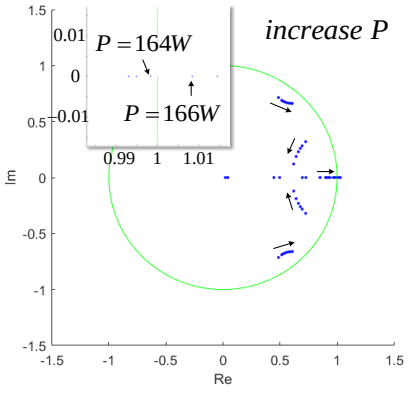

(b)

Fig. 9 Loci of eigenvalues by varying P.
(a)P from 40W to 15W (b)P from 140W to 170W

TABLE V

P/W	absolute value of eigenvalues	Remarks
31	0.9994	Unstable
32	0.9997	Unstable
33	0.9999	Unstable
34	1.0003	Stable
35	1.0006	Stable
36	1.0009	Stable
37	1.0012	Stable

TABLE VI

P/W	absolute value of eigenvalues	Remarks
158	0.9638	Stable
160	0.9733	Stable
162	0.9899	Stable
164	0.9997	Stable
166	1.0088	Unstable
168	1.0143	Unstable
170	1.0286	Unstable

In this study, the cut-off frequency f_c of the input filter is set to 2.5kHz. Therefore, the relation between L_1 and C_1 is as follows.

$$C_1 = \left(\frac{1}{2\pi f_c}\right)^2 / L_1 \tag{13}$$

Loci of eigenvalues when L_1 increased from 0.1mH to 0.6mH are plotted and shown in Fig. 10, where P=100W, k_p =0.45, k_2 =-0.01. As seen, Hopf bifurcation occurs in the system when L_1 = 0.37mH. In addition, loci of eigenvalues move outward as L_1 increases, which means that large L_1 may cause instability. Therefore, a small inductor is preferred in input filter design.

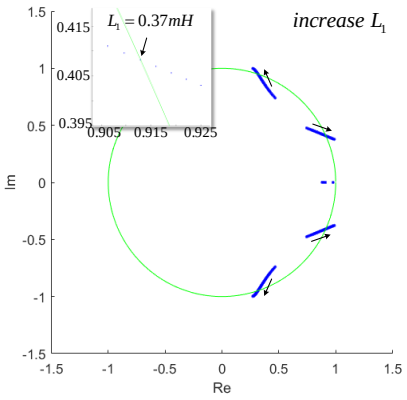

Fig. 10 Loci of eigenvalues by varying L_1 and C_1. (L_1 from 0.1mH to 0.6mH)

TABLE VI

L_1/mH	absolute value of eigenvalues	Remarks
0.34	0.9921	Stable
0.35	0.9954	Stable
0.36	0.9983	Stable
0.37	0.9997	Stable
0.38	1.0008	Unstable
0.39	1.0017	Unstable
0.40	1.0025	Unstable

This article has been accepted for publication in a future issue of this journal, but has not been fully edited. Content may change prior to final publication. Citation information: DOI 10.1109/JESTIE.2021.3093249, IEEE Journal of Emerging and Selected Topics in Industrial Electronics

C. Margin of Stability Curve

To guide the controller design of DAB intuitively, stable boundaries are given in this section. Fig. 11 shows the 3-dimensional stable boundary of k_p, k_2, and P, where the points right above the stable boundary surface are stable.

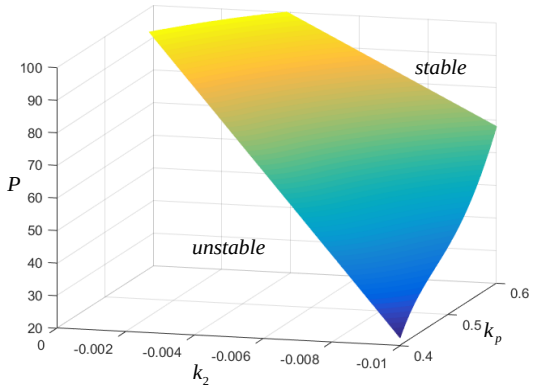

Fig. 11. stable boundary of k_p, k_2, and P.

To show more details of Fig. 11, two 2-dimensional stable boundary pictures are plotted. Fig. 12 and Fig. 13 show the stability boundary of k_2 and k_p when P=100W and the stability boundary of P and k_p when k_2=-0.01, respectively.

To select control parameters, stability and dynamic response requirements must be considered simultaneously. For example, to select a proper k_p the following steps can be taken. First, the feasible range of k_p can be determined according to Fig. 11. It is clear that the larger k_p is, the faster the response is. Thus, a larger k_p but less than its maximum allowable value is selected in the second step. Sometimes, trial and error will be taken according to practical requirements.

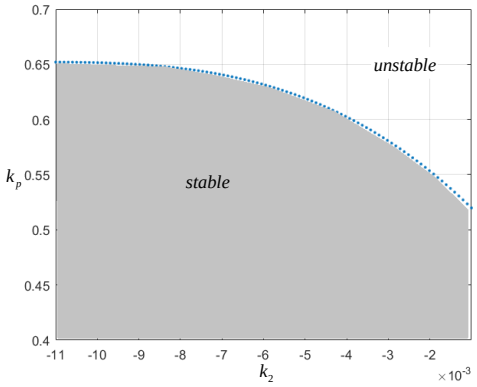

Fig. 12. The stability boundary of k_p and k_2. (P = 100W)

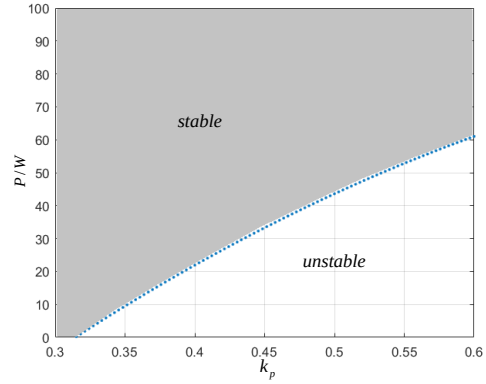

Fig. 13. The stability boundary of P and k_p. (k_2= -0.01)

D. Comparison with Different Models

Besides the switching function model, the reduced-order average model is also introduced in section II. In this section, the confidence level in stability prediction will be tested by contrast.

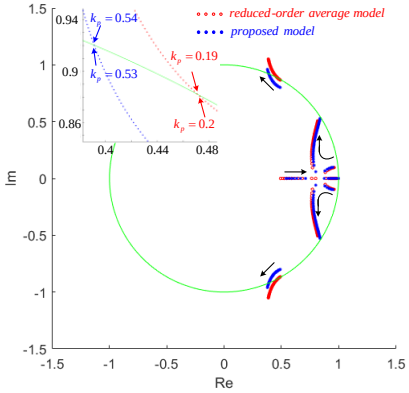

Fig. 14. eigenvalues loci of reduced-order average model and proposed model

The eigenvalue loci of the reduced-order average model by changing k_p are shown in Fig. 14. The parameter setting is completely the same as before. Compared to Fig. 7, it is found that both the eigenvalue loci move away the unit circle with increasing k_p, but the eigenvalue loci under different models are different. As seen from Fig. 14, the calculated bifurcation point based on the equivalent average model is k_p=0.2, while the proposed model predicts that the bifurcation point occurs at k_p=0.54. The rest part of this paper verifies the bifurcation point occurs at k_p=0.54 by simulations and experiments. Thus, the confidence level in stability prediction based on the equivalent average model is low, its predicting outcomes are too conservative.

E. Comparison with DAB without input filter and CPL

For comparison, similar analyses for the DAB without input filter and CPL are carried out. It is noted that the output voltage reference, output power and the other parameters are the same as those in this study.

The bifurcation diagram with P=100W, k_2=-0.017 is plotted in Fig. 15, where k_p is the bifurcation parameter. Compared with Fig.4, it is clear that control parameter k_p has a wider stable range in the DAB without input filter and constant power load. The bifurcation diagram with k_p=0.45, k_2=-0.01, using P as the bifurcation parameter is shown in Fig. 16. As seen, there is no bifurcation over a wide output power range. Compared with Fig. 6, Hopf bifurcations under light load can be found in the DAB with input filter and CPL.

Based on the comparisons above, it can be concluded that the dynamic behavior of DAB with input filters and CPL changes significantly compared to the existing ones. Moreover, it is easier for the DAB with input filters and CPL to lose its stability. Because in practical application input filters for DAB are usually installed, the stability analysis in this paper is important and meaningful to the design of the DAB.

This article has been accepted for publication in a future issue of this journal, but has not been fully edited. Content may change prior to final publication. Citation information: DOI 10.1109/JESTIE.2021.3093249, IEEE Journal of Emerging and Selected Topics in Industrial Electronics

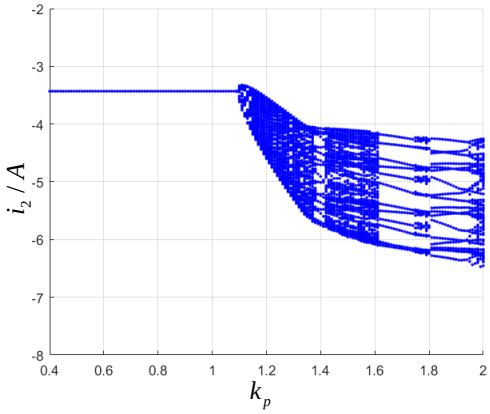

Fig. 15 Bifurcation diagram for i_2 using k_p as the bifurcation parameter (P=100W, k2=-0.017, without input filter and CPL)

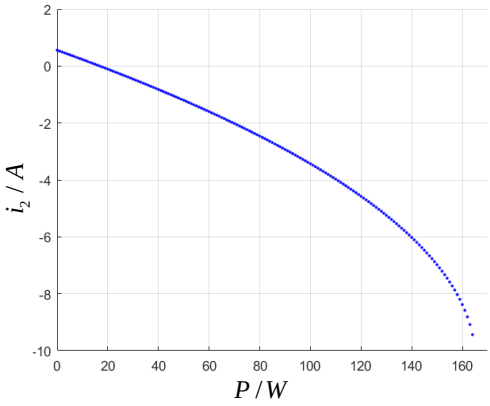

Fig. 16 Bifurcation diagram for i_2 using P as the bifurcation parameter. (k_p=0.45, k_2=-0.01, without input filter and CPL)

IV. Simulation Verifications

In order to verify the theoretical analysis, simulations are carried out in this section. The model of the system is built in MATLAB/Simulink. System parameters are same as those in Table. I. The control delay is equal to the sampling period.

To show the transient performance of the converter, two experiments are performed. Fig. 17 shows the dynamic response under step changes of load (40W to 140W) and Fig. 16 shows the dynamic response under step changes of supply voltage E (25V to 35V) in the case of k_p=0.45, k_2=-0.01 and P=100W. As seen, the converter can return or reach to the steady state after disturbances quickly.

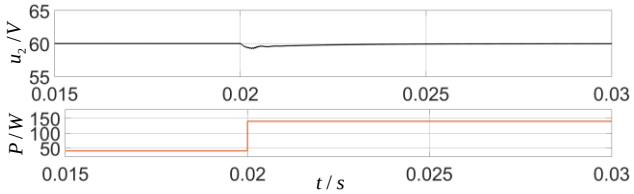

Fig.17 the dynamic performance under step changes of loads. (40W to 140W).

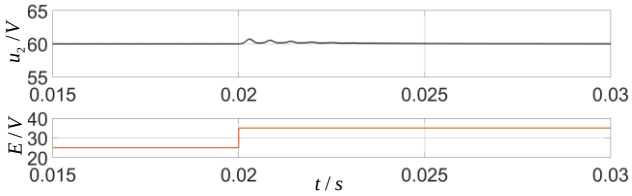

Fig.18 the dynamic performance under step changes in supply voltage E. (30V to 40V).

Fig. 19(a) shows the leakage inductance current waveform in the case of k_p=0.52, k_2=-0.017 and P=100W. Fig. 19(b) shows the leakage inductance current waveform when k_p=0.55, k_2=-0.017 and P=100W. Comparing the results in Fig. 19, it is observed that the system is stable when k_p=0.52, and it loses stability when k_p=0.55. Clearly, the simulation results are consistent with the analysis of Fig. 7.

Fig. 20(a) shows the simulation result when k_2=-0.016, k_p=0.45 and P=100W. And Fig. 20 (b) illustrates the result when k_2 =-0.019. As seen, the converter works normally when k_2=-0.016, while it becomes unstable when k_2 =-0.019, which is in agreement with the analysis of Fig. 8.

Fig. 21 shows the simulation results under different values of load power with k_p =0.45 and k_2 =-0.01. According to Fig.21, the converter is stable when P=35W and is unstable when P=30W, which is in agreement with the analysis of Fig. 9.

Fig. 22 shows the simulation results under different values of L_1 and C_1 with P = 100W, k_p =0.45, k_2 =-0.01 and f_c =2500Hz. According to Fig. 22, the converter is stable when L_1=0.35mH and is unstable when L_1=0.4mH, which is in agreement with the analysis of Fig. 10.

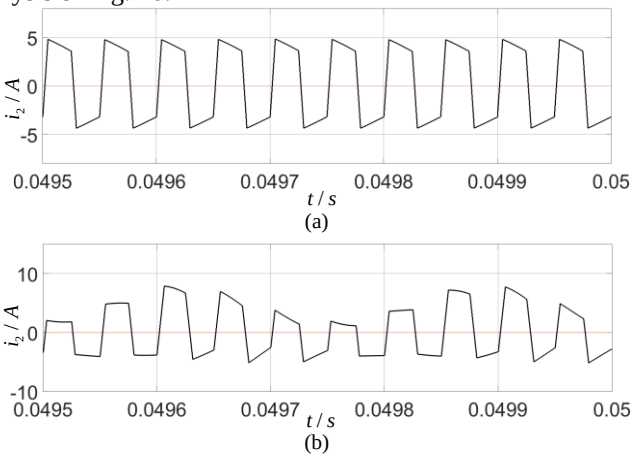

Fig. 19. Simulation results (k_2=-0.017 and P=100W). (a) Inductor current when k_p =0.52 (b) Inductor current when k_p =0.55

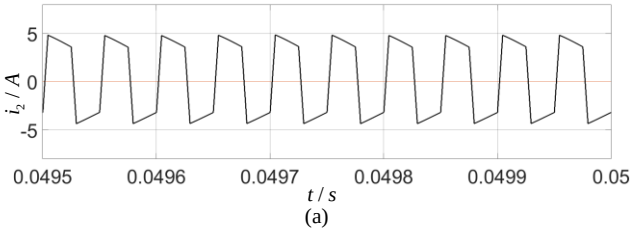

This article has been accepted for publication in a future issue of this journal, but has not been fully edited. Content may change prior to final publication. Citation information: DOI 10.1109/JESTIE.2021.3093249, IEEE Journal of Emerging and Selected Topics in Industrial Electronics

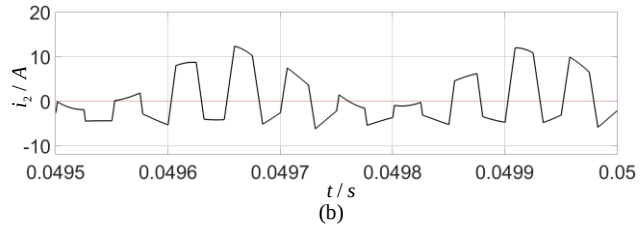

(b)

Fig. 20. Simulation results (k_p=0.45 and P=100W). (a) Inductor current when k_2=-0.016 (b) Inductor current when k_2=-0.019

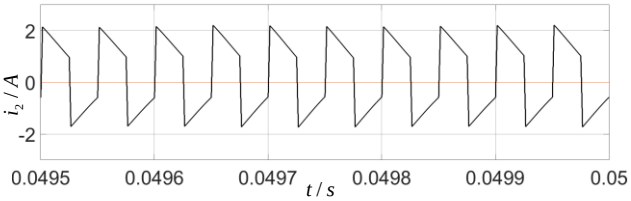

(a)

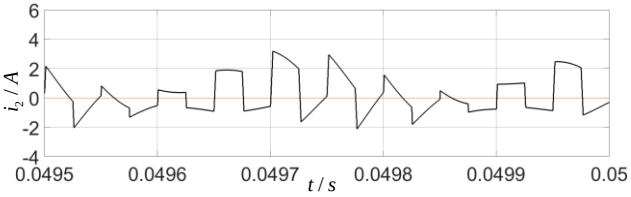

(b)

Fig. 21. Simulation results (k_p =0.45 and k_2 =-0.01). (a) Inductor current when P = 35W (b) Inductor current when P = 30W

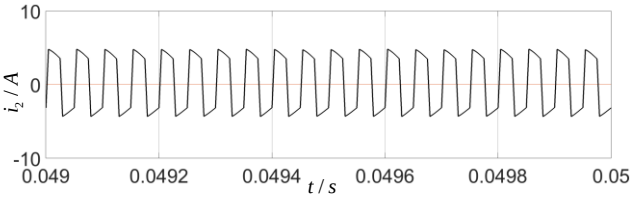

(a)

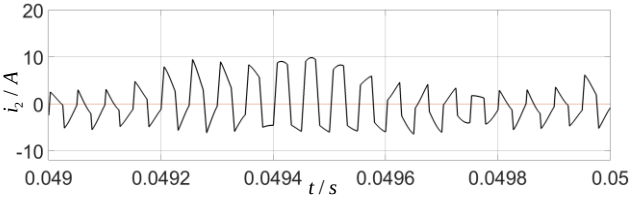

(b)

Fig. 22. Simulation results (P = 100W, k_p =0.45 and k_2 =-0.01). (a)Inductor current when L_1=0.35mH (b) Inductor current when L_1=0.4mH

V. Experimental Validation

Based on the circuit structure shown in Fig. 1 and parameters in Table I, an experimental prototype shown in Fig. 23 has been constructed to validate the theoretical and numerical results before. An electronic load IT8733B is used to emulate the constant power load. TMS320F28069 controller is used to implement the control laws. Power MOSFETs (FCH072N60F) are used as semiconductor switches $S_1 - S_8$.

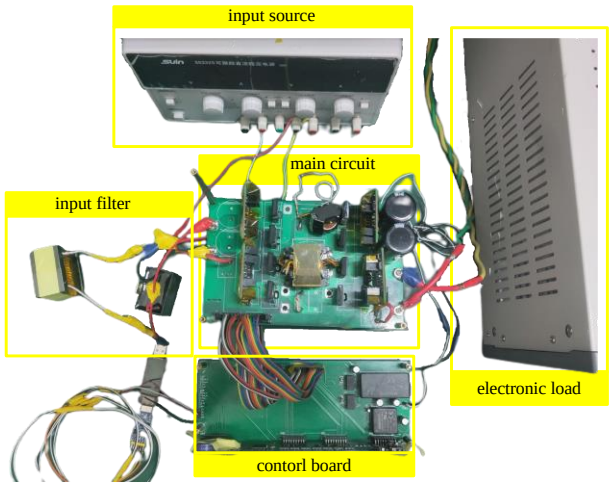

Fig. 23. Photograph of the experimental prototype.

Firstly, The effect of different k_p on stability is tested. Fig. 24(a) shows the experimental results in the case of k_p=0.5, k_2=-0.017 and P=100W. As seen, both input voltage u_1 and output voltage u_2 are constant, and the waveform of the leakage inductance current i_2 is a periodic trajectory. Fig. 24(b) shows

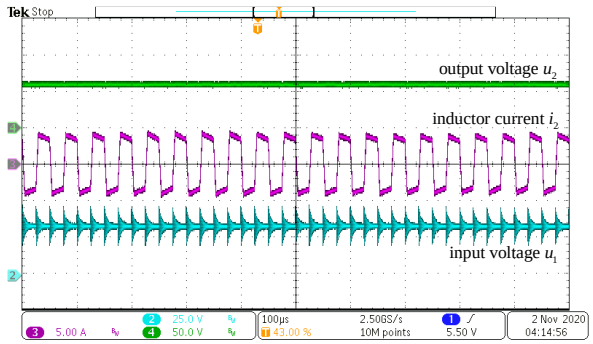

(a)

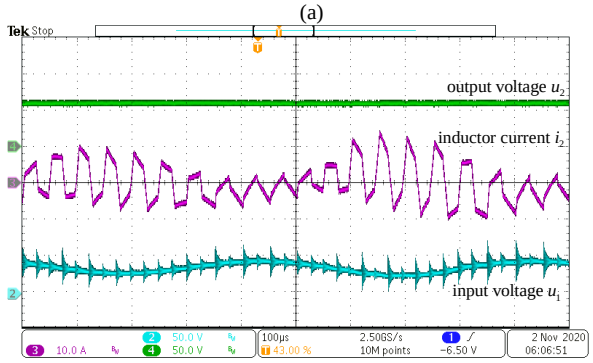

(b)

Fig. 24. Experimental results (k_2=-0.01 and P=100W). (a) Inductor current when k_p =0.5 (b) Inductor current when k_p =0.6

This article has been accepted for publication in a future issue of this journal, but has not been fully edited. Content may change prior to final publication. Citation information: DOI 10.1109/JESTIE.2021.3093249, IEEE Journal of Emerging and Selected Topics in Industrial Electronics

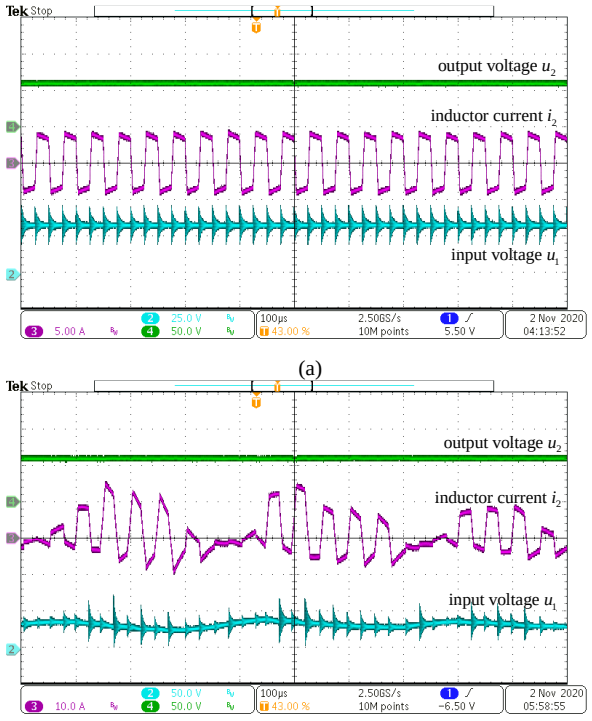

Fig. 25. Experimental results (k_p =0.45 and P=100W). (a) Inductor current when k_2=-0.01 (b) Inductor current when k_2=-0.02

the experimental results in the case of k_p=0.6, k_2=-0.017 and P=100W. It is clear that the converter has lost its stability and both input voltage u_1 and inductance current i_2 are oscillating. The experimental results consist with the simulation analysis of Fig. 19.

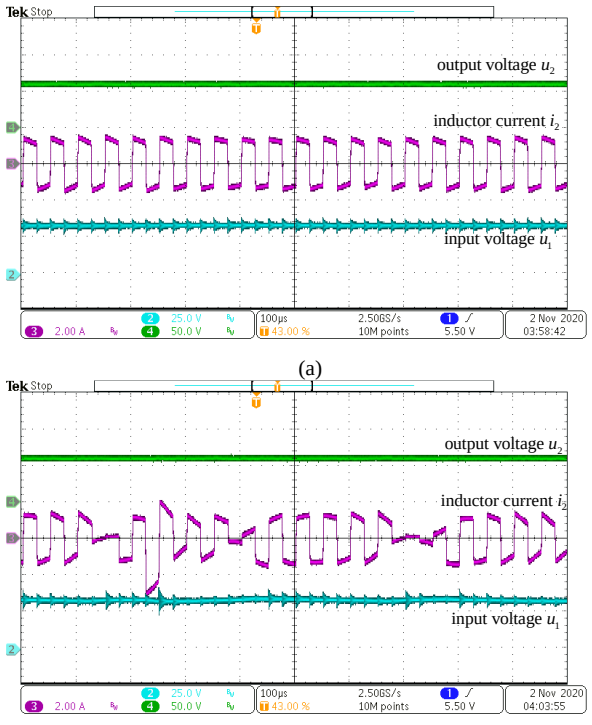

Fig. 26. Experimental results (k_2=-0.01 and k_p =0.45). (a) Inductor current when P =40W (b) Inductor current when P=30W

Then, the effect of different k_2 on stability is tested. Fig. 25(a) shows the experimental results in the case of k_p=0.45, k_2=-0.01 and P=100W. Fig. 25(b) illustrates the experimental results in the case of k_p=0.45, k_2=-0.02 and P=100W. Comparing the results in Fig. 18, it is found that the system is stable when k_2=-0.01. It loses stability when k_2=-0.02, which is in agreement with the result of Fig. 20.

At last, the effect of different P on stability is tested. Fig. 26 shows the experimental results under different values of load power with k_p =0.45 and k_2 =-0.01. As seen, the converter works normally when P=40W, while it becomes unstable when P =30W, which is same as the conclusions from Fig. 21.

Overall, the experimental waveforms exhibit the same dynamical behavior as the analytical and simulation results.

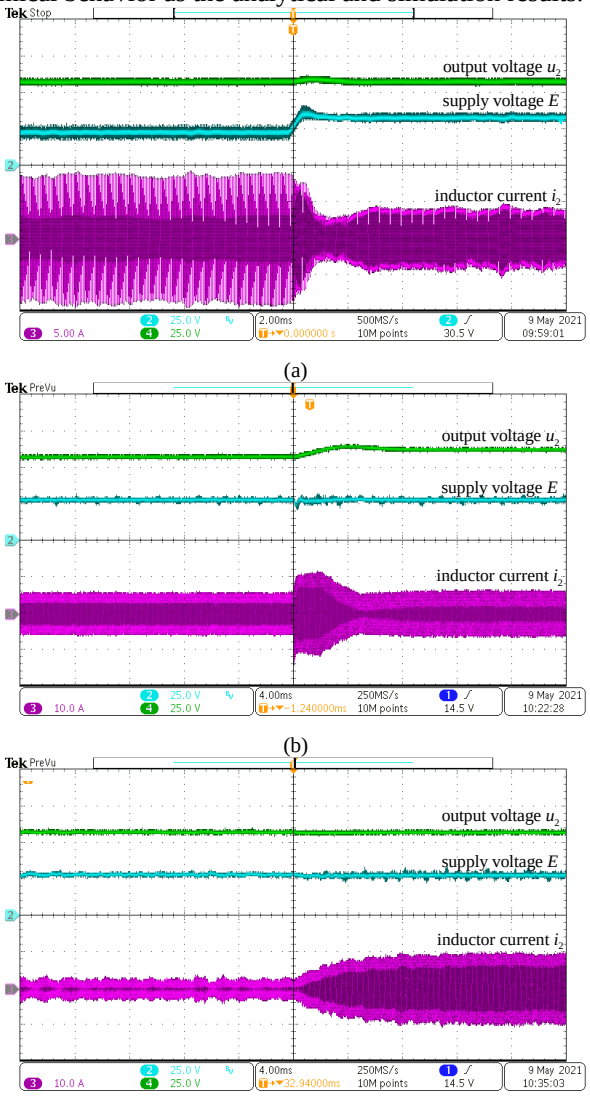

Fig. 27. Experimental results (k_p =0.45, k_2=-0.01 and P=100W). (a) supply voltage changing from 25V to 35V (b) output voltage reference changing from 60V to 65V. (c) P changing from 40W to 140W.

To demonstrate the stability of the DAB system under disturbances, the experimental results for dynamic response are given. Fig. 27(a) shows the experimental results when supply voltage changes from 25V to 35V, which indicates that the system has good ability of disturbance rejection. Fig. 27(b)

shows the response of the system when output voltage reference changes from 60V to 65V. And Fig. 27(c) shows the experimental results when the constant power load changes from 40W to 140W. As seen, the system remains stable after step changes of parameters or references and the output voltage could converge to its given value quickly.

VI. Conclusion

Fast scale stability analysis of DAB converter with input filter under constant power load conditions are carried out. A discrete-time model is derived for the digitally controlled DAB converter. Compared to the reduced order average model, the proposed model takes into account the dynamic of inductance current i_2 of DAB, which is more accurate. In addition, the influence of the delay caused by the digital controller on the system stability considered. Based on the model, bifurcation diagrams and Jacobian matrix analysis are carried out. The analysis results indicate that Hopf bifurcation and saddle-node bifurcation take place in the converter when varying the control and load or input filter parameters. For example, increasing k_p will improve the control bandwidth of output voltage, but a Hopf bifurcation is found for large k_p. Two Hopf bifurcations points are found by changing k_2. Thus, k_2 must lie in a proper interval for stability requirement. A Hopf bifurcation is found for a small CPL, and a saddle-node bifurcation appears in the converter for a large CPL. In all, the results obtained in this study provide a guideline for controller and circuit design of DAB converters to avoid all kinds of undesired bifurcations.

Reference

[1] S. Banerjee and G. C. Verghese, *Nonlinear phenomena in power electronics — Attractors, Bifurcations, Chaos, and Nonlinear Control*. New York : IEEE Press, 2001.

[2] C. K. Tse, *Complex Behavior of Switching Power Converters*. New York : CRC Press, 2003.

[3] Z. Biao, S. Qiang, L. Wenhua, and S. Yandong, "Overview of dual-activebridge isolated bidirectional DC-DC converter for high-frequency-link power-conversion system," *IEEE Trans. Power Electron.*, vol. 29, no. 8, pp. 4091–4106, Aug. 2014.

[4] L. Shi, W. Lei, Z. Li, J. Huang, Y. Cui, and Y. Wang, "Bilinear discrete-time modeling and stability analysis of the digitally controlled dual active bridge converter," *IEEE Trans. Power Electron.*, vol. 32, no. 11, pp. 8787–8799, Nov. 2017.

[5] Ling Shi, Wanjun Lei, Jun Huang, Zhuoqiang Li, Yao Cui and Yue Wang, "Full discrete-time modeling and stability analysis of the digital controlled dual active bridge converter," *2016 IEEE 8th International Power Electronics and Motion Control Conference (IPEMC-ECCE Asia)*, Hefei, China, 2016, pp. 3813-3817.

[6] H. Krishnamurthy and R. Ayyanar, "Stability analysis of cascaded converters for bidirectional power flow applications," *in Proc. IEEE 30th Int. Telecommun. Energy Conf.*, Sep. 2008, pp. 1–8.

[7] G. Gao, W. Lei, Q. Tang, Z. Xiao, X. Hu, and Y. Wang." Decomposed Discrete-Time Model and Multiscale Oscillations Analysis of the DAB Converter," *IEEE Trans. Power Electron.*, vol. 35, no. 9, sept. 2020.

[8] R. D. Middlebrook and S. Cuk, "A general unified approach to modelling switching-converter power stages," *in Proc. IEEE Power Electron. Specialists Conf.*, 1976, pp. 18–34.

[9] A. Forsyth and S. V. Mollov, "Modelling and control of DC-DC converters," *Power Eng. J.*, vol. 12, no. 5, pp. 229–236, Oct. 1998.

[10] S. R. Sanders, J. M. Noworolski, X. Z. Liu, and G. C. Verghese, "Generalized averaging method for power conversion circuits," *IEEE Transactions on Power Electronics*, vol. 6, no. 2, pp. 251–259, 1991.

[11] V. A. Caliskan, O. C. Verghese, and A. M. Stankovic, "Multifrequency averaging of DC/DC converters," *IEEE Transactions on Power Electronics*, vol. 14, no. 1, pp. 124–133, 1999.

[12] Z. Li, Y. Wang, L. Shi, J. Huang, Y. Cui, and W. Lei, "Generalized averaging modeling and control strategy for three-phase dual-active bridge DC-DC converters with three control variables," *in 2017 IEEE Applied Power Electronics Conference and Exposition (APEC)*, 2017, pp. 1078–1084.

[13] Hengsi Qin and J. W. Kimball, "Generalized Average Modeling of Dual Active Bridge DC–DC Converter," *IEEE Transactions on Power Electronics*, vol. 27, no. 4, pp. 2078–2084, Apr. 2012.

[14] H. Bai, Z. Nie, and C. C. Mi, "Experimental comparison of traditional phase-shift, dual-phase-shift, and model-based control of isolated bidirectional DC–DC converters," *IEEE Trans. Power Electron.*, vol. 25, no. 6, pp. 1444–1449, Jun. 2010.

[15] B. Hua, M. Chunting, W. Chongwu, and S. Gargies, "The dynamic model and hybrid phase-shift control of a dual-active-bridge converter," *in Proc. 34th Annu. Conf. IEEE Ind. Electron.*, Nov. 2008, pp. 2840–2845.

[16] K. Zhang, Z. Shan, and J. Jatskevich, "Large- and small-signal average value modeling of dual-active-bridge DC–DC converter considering power losses," *IEEE Trans. Power Electron.*, vol. 32, no. 3, pp. 1964–1974, Mar. 2017.

[17] J. Guacaneme, G. Garcerá, E. Figueres, I. Patrao, and R. González-Medina, "Dynamic modeling of a dual active bridge DC to DC converter with average current control and load-current feed-forward," *Int. J. Circuit Theory Appl.*, vol. 43, no. 10, pp. 1311–1332, 2015, doi: 10.1002/cta.2012.

[18] D. Maksimovic and R. Zane, "Small-signal discrete-time modeling of digitally controlled PWM converters," *IEEE Trans. Power Electron.*, vol. 22, no. 6, pp. 2552–2556, Nov. 2007.

[19] C. Zhao, S. D. Round, and J. W. Kolar, "Full-order averaging modelling of zero-voltage-switching phase-shift bidirectional DC-DC converters," *IET Power Electron.*, vol. 3, no. 3, pp. 400–410, 2010.

[20] D. Costinett, R. Zane, and D. Maksimovic, "Discrete time modeling of output disturbances in the dual active bridge converter," *in Proc. IEEE Appl. Power Electron. Conf. Expo.*, 2014, pp. 1171–1177.

[21] D. Costinett, "Reduced order discrete time modeling of ZVS transition dynamics in the dual active bridge converter," *in Proc. IEEE Appl. Power Electron. Conf. Expo.*, 2015, pp. 365–370.

[22] D. Costinett, R. Zane and D. Maksimović, "Discrete-time small-signal modeling of a 1 MHz efficiency-optimized dual active bridge converter with varying load," *2012 IEEE 13th Workshop on Control and Modeling for Power Electronics (COMPEL)*, Kyoto, Japan, 2012, pp. 1-7.

[23] Daniel M. Mitchell, "Power Line Filter Design Considerations For dc-dc Converters," *IEEE Industry Applications Magazine*, Vol. 5, no. 6, pp.16-20, Nov/Dec 1999.

[24] M. Su, Z. Liu, Y. Sun, H. Han, and X. Hou, "Stability Analysis and Stabilization methods of DC Microgrid with Multiple Parallel-Connected DC-DC Converters loaded by CPLs," *IEEE Trans. Smart Grid.*, vol. 9, no.1, pp.132-142, Jan. 2018.

[25] A. Emadi, A. Khaligh, C. H. Rivetta, and G. A. Williamson, "Constant power loads and negative impedance instability in automotive systems: Definition, modeling, stability, and control of power electronic converters and motor drives," *IEEE Trans. Veh. Technol.*, vol. 55, no. 4, pp. 1112–1125, Jul. 2006.

[26] M. Huang, H. Ji, J. Sun, L. Wei, and X. Zha, "Bifurcation-Based Stability Analysis of Photovoltaic-Battery Hybrid Power System," *IEEE Journal of Emerging and Selected Topics in Power Electronics*, vol. 5, no. 3, pp. 1055–1067, Sept. 2017.

[27] M. Zhang, Y. Li, F. Liu, L. Luo, Y. Cao and M. Shahidehpour, "Voltage Stability Analysis and Sliding-Mode Control Method for Rectifier in DC Systems With Constant Power Loads," *IEEE Journal of Emerging and Selected Topics in Power Electronics*, vol. 5, no. 4, pp.1621-1630, Dec. 2017.

[28] C. Mi, H. Bai, C. Wang and S. Gargies, "Operation, design and control of dual H-bridge-based isolated bidirectional DC–DC converter," *IET Power Electron.*, Vol. 1, No. 4, pp. 507– 517, 2008.

[29] A. El Aroudi, R. Haroun, M. Al-Numay, J. Calvente, and R. Giral, "Fast-Scale Stability Analysis of a DC-DC Boost Converter with a Constant Power Load," *IEEE Journal of Emerging and Selected Topics in Power Electronics*, DOI 10.1109/JESTPE.2019.2960564.

[30] A. Pal, S. Kapat, K. Jha and A. Tiwari, "Discrete-time framework for digital control design in a high-frequency dual active bridge converter," *2018 IEEE Applied Power Electronics Conference and Exposition*

(APEC), San Antonio, TX, USA, 2018, pp. 2264-2270.

Yao Sun was born in Hunan, China, in 1981. He received the B.S., M.S. and Ph.D. degrees from Central South University, Changsha, China, in 2004, 2007 and 2010, respectively. He has been a Professor with the School of Automation, Central South University, China.

His research interests include matrix converter, micro-grid and wind energy conversion system.

Shutian Yan was born in Hunan, China, in 1997. He received the B.S. degree in electrical engineering from Central South University, China, in 2018, where he is currently pursuing the M.S. degree in electrical engineering.

His research interests include modeling and stability of power electronics systems.

Guo Xu (M'15) received the B.S. degree in electrical engineering and automation and the Ph.D. degree from the Beijing Institute of Technology, Beijing, China, in 2012 and 2018, respectively. From 2016 to 2017, he was a Visiting Student with the Center for Power Electronics System, Virginia Polytechnic Institute and State University, Blacksburg, VA, USA. Since 2018, he has been with the School of Automation, Central South University, Changsha, China, where he is currently an Associate Professor.

His research interests include modeling and control of power electronics converters, high-efficiency power conversion, and magnetic integration in power converters.

Guoliang Deng was born in Guangdong, China, in 1995. He received the B.S. degree in electrical engineering and automation from Central South University, Changsha, China, in 2018, where he is currently working toward the Master degree.

His research interests include modeling and control of power electronics converters and high-efficiency power conversion.

Mei Su was born in Hunan, China, in 1967. She received the B.S. and M.S. degrees in industrial automation, and Ph.D. degree in control science and engineering from the School of Information Science and Engineering, Central South University, Changsha, China, in 1989, 1992, and 2005, respectively. She has been a Full Professor with the School of Automation, Central South University. She is currently an Associate Editor of the IEEE Transactions on Power Electronics.

Her research interests include matrix converter, adjustable speed drives, and wind energy conversion system.